

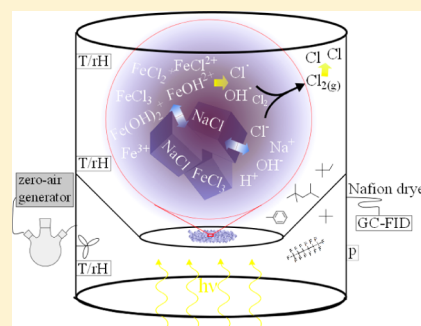
Iron(III)-Induced Activation of Chloride and Bromide from Modeled Salt Pans

Julian Wittmer, Sergej Bleicher, and Cornelius Zetzsch*

Atmospheric Chemistry Research Unit, BayCEER, University of Bayreuth, Dr. Hans-Frisch Strasse 1-3, 95448 Bayreuth, Germany

S Supporting Information

ABSTRACT: The photochemistry of halides in sea spray aerosol, on salt pans, and on other salty surfaces leads to a formation of reactive halogen species. We investigated the photochemical formation of atomic chlorine (Cl) and bromine (Br) in the gas phase in the presence of laboratory-modeled salt pans consisting of sodium chloride doped with iron(III) chloride hexahydrate (0.5 and 2 wt %). The samples were spread on a Teflon sheet and exposed to simulated sunlight in a Teflon smog chamber in purified, humidified air in the presence of a test mixture of hydrocarbons at the ppb level to determine Cl, Br, and OH formation by the radical clock method. Driven by the photolytic reduction of Fe(III) to Fe(II), the production rates of the Fe(III)-doped NaCl salt samples (up to 10^7 atoms $\text{cm}^{-3} \text{s}^{-1}$) exceeded the release of Cl above a pure NaCl sample by more than an order of magnitude in an initially O_3 -free environment at low NO_x . In bromide-doped samples (0.5 wt % NaBr), a part of the Cl release was replaced by Br when Fe(III) was present. Additions of sodium sulfate, sodium oxalate, oxalic acid, and catechol to NaCl/ FeCl_3 samples were found to restrain the activation of chloride.



1. INTRODUCTION

Besides the hydroxyl radical (OH), chlorine atoms (Cl) are an important oxidant in the troposphere, particularly in marine environments.^{1–4} Despite the importance of Cl for the ozone destruction mechanism in the stratosphere,^{5,6} the multifaceted role of atomic Cl in the lower part of the atmosphere as a depletion reagent for ozone or as an initiator of photochemistry in the early morning was rather underestimated and came into focus in the last 2 decades.^{1,7} Newer studies show an impact of reactive halogen species from the occurrence of nitryl chloride (ClNO_2) even in continental regions.^{8,9} Chlorine atoms are an effective consumer of volatile organic compounds (VOCs) and also influence the cycles of ozone (O_3) and nitrogen oxides (NO_x). Among the VOCs, the short-lived greenhouse gas methane (CH_4) is of major interest in climate research to date. Atomic Cl has a 16 times faster reaction rate constant toward methane in comparison to hydroxyl radicals at 298 K.¹⁰ Moreover, the behavior of the isotope enrichment, $\delta^{13}\text{C}$, of CH_4 in the tropospheric background can be ascribed to the reaction with atomic Cl representing a sink for CH_4 of 19 Tg yr^{-1} that corresponds to 3.3% of the total CH_4 .^{11–13} Levine et al.¹⁴ suggest that Cl could have been responsible for about 10% of the glacial–interglacial change in the isotopic composition of CH_4 . A main question is therefore to determine and quantify the sources of atomic chlorine and their dependencies. The natural processes that are responsible for the activation of chloride in the liquid or solid phase into a gaseous form are only partly understood, and decisive inorganic halogen species (e.g., ClNO , BrNO , ClONO_2 , BrONO_2 , ClOH , HOBr) have not been detected yet in the troposphere,¹⁵ although the dependence on various parameters like pH,¹⁶ bromine

content,¹⁷ and the concentrations of NO_x and O_3 ^{18,19} has been investigated.

High concentrations of reactive halogen species were observed in sea-salt-influenced environments, such as the Arctic. For example, Jobson et al. calculated concentrations of $(0.39–7.7) \times 10^4$ Cl atoms cm^{-3} and $(0.3–6.1) \times 10^7$ Br atoms cm^{-3} for 1 day during their campaign at Alert, Northwest Territories,²⁰ by employing the radical clock technique during ozone depletion events.^{17,18,21} Combined with the measured concentrations of $\text{C}_2–\text{C}_6$ hydrocarbons and their reaction rates toward Cl and Br given by Jobson et al.,²⁰ this requires production rates of $(0.2–3.6) \times 10^5$ Cl atoms $\text{cm}^{-3} \text{s}^{-1}$ and $(0.2–3.3) \times 10^5$ Br atoms $\text{cm}^{-3} \text{s}^{-1}$ at least (not considering the contributions of other trace gases to the total reactivity of the atmosphere against Cl and Br). Furthermore, several studies detected reactive halogen species (including the molecular halogens) on coastal sites of the Arctic^{3,22–25} above salt lakes and salt-covered areas such as the Dead Sea, Israel, or the Great Salt Lake, UT (U.S.A.)^{26–28} and also in volcanic plumes.^{29,30}

More than a century ago, Eder³¹ observed a catalytic effect of iron on chloride activation in solid salt and in the liquid phase when exposed to sunlight. In particular, the formation of iron(II) and aqueous $\text{Cl}_2^{\bullet-}$ radicals (due to the photodecomposition of iron(III) complexes in chloride-containing solutions) has been manifested by several studies^{32–36} that mainly concentrate on the detection of atomic chlorine formed

Special Issue: Mario Molina Festschrift

Received: August 7, 2014

Revised: September 18, 2014

in the aqueous phase but also observed the degassing of chlorine molecules (Cl_2) formed via combination of $\text{Cl}_2^{\bullet-}$.³⁷ The speciation and photochemistry in the quasi-liquid microlayer (QLM) on the salt crystals are decisive for the halogen release. Depending on the composition of the salt and the humidity, water adsorbs on the crystals and forms and modifies the thickness and properties of the QLM.^{38,39} The photolytic reduction of Fe(III) to Fe(II) plays a key role in the photo-Fenton reaction, together with hydrogen peroxide (H_2O_2), that is responsible for the reoxidation to Fe(III). However, the photo-Fenton reaction is inhibited at high salinity due to the formation of Fe–Cl complexes and the scavenging of OH radicals by Cl^- , both forming the less reactive $\text{Cl}_2^{\bullet-}$ radical anion and lowering the combination of OH^\bullet to H_2O_2 .^{35,40}

The present study deals with the photoinduced formation and release of Cl_2 , BrCl , and Br_2 from humidified salts (in an O_3 -free environment at low NO_x), detected indirectly in the form of Cl and Br atoms. In order to reproduce natural processes, the effects of several inorganic (Mg^{2+} , Br^- , SO_4^{2-}) and organic ($\text{C}_2\text{O}_4^{2-}$, $\text{C}_6\text{H}_6\text{O}_2$) constituents of natural salts are investigated in this work. In particular, an inhibiting impact of sulfate on the photo-Fenton reaction is known.³⁴ Moreover, bromide, which is far easier to oxidize than chloride, stimulates the activation of chloride.^{16,17} Even small amounts of bromide have a high impact on the chloride chemistry, whereas the impact of bromide on the iron-induced chloride activation is still unclear and experimentally investigated in this work for the first time. Hypobromous acid (HOBr) combines with Br^- to form Br_2 but may also form bromine monochloride (BrCl) in the predominant presence of Cl^- . Br_2 and BrCl are released to the gas phase, depending on the pH, and are photolyzed by sunlight to atomic Br and Cl, respectively. Organic compounds like oxalic acid ($\text{H}_2\text{C}_2\text{O}_4$) or catechol ($\text{C}_6\text{H}_6\text{O}_2$) are known to influence iron ions by complexation^{41,42} and thus intervene in the photoproduction of aqueous halogens and OH radicals.⁴³ Additionally, oxalate acts as a scavenger of OH^\bullet .⁴⁴ The iron–catechol complexes are strongly colored and thus change the light-absorbing properties of the salt samples.^{45,46}

2. EXPERIMENTAL SETUP AND METHODS

2.1. Smog Chamber and Its Analytical Instrumentation. Measurements are performed in a cylindrical smog chamber made of Teflon film (FEP 200A, DuPont) that is fixed on three aluminum rings of 1.33 m diameter and combines two widths of the Teflon film to obtain a height of 2.5 m. This leads to a volume of more than 3500 L (slightly dependent on the internal pressure) and a surface to volume ratio of 3.8 m^{-1} .⁴⁷ The whole construction is suspended above an IR filter (2 cm of deionized water), a UV filter (3 mm of borosilicate glass), and bifocal reflectors with seven medium pressure arc lamps (Osram HMI, 1.2 kW each) to reproduce the actinic flux of the summer sun at 50° latitude.⁴⁸ Because the lamps have a heat-up time of 3 min until they attain their full intensity, they were covered during this time and rapidly uncovered at the beginning of the experiment.

To replenish the air consumption of the gas analyzers and warrant the zero air environment, a slight overpressure of 0.5–2 Pa (differential pressure sensor, Kalinsky Elektronik DS1) is maintained by a continuous flow of hydrocarbon-free zero air (zero-air-generator, cmc instruments, <1 ppb O_3 , <0.5 ppb NO_x , <100 ppb CH_4) controlled by a mass flow controller (Tylan FC2910). Before flowing into the chamber, the zero air

is humidified by a three-necked flask that is filled with bidistilled water and placed on a heater. In this way, the humidity can be adjusted by the water temperature in the flask. All experiments in this study were conducted at constant conditions at 20°C and 55–60% relative humidity (RH), which was monitored by sensors (Driesen + Kern DKRF400X-P) at three levels of the chamber (top, middle, and bottom). Continuous mixing was achieved by a custom-built fan (made of PTFE-Teflon), placed directly below the zero air inlet to achieve mixing times of 3–4 min. Furthermore, the smog chamber was equipped with an analyzer for NO (EcoPhysics, CLD 88p), coupled with a photolytic converter for NO_x (EcoPhysics, PLC 860), and with two O_3 analyzers (UPK 8001 and Thermo Fisher Scientific 49i). A more detailed description of the smog chamber and its analytical instrumentation can be found elsewhere.^{47,48}

2.2. Sample Preparation. The salt pans were prepared by solving the desired amount of compound in 500 mL of bidistilled water under gentle warming (below 50°C) to allow complete dissolution. In order to obtain a crystallized salt sample, the turbid brine, containing various brownish iron(III) species as the hydrolysis product,⁴⁹ was dried on a Teflon sheet (FEP 200A, DuPont) in a wide beaker (diameter 225 mm) at 50°C for at least 70 h under a constant zero air flow. The crust above the brine was broken every 24 h in order to achieve total dryness. Afterward, the residue was either milled in a ball mill (Retsch MM 2, Haan, Germany) or ground in a household salt mill or used as an untreated polycrystalline salt, depending on the hygroscopicity and thus the stickiness of the salt mixture. Each sample was spread on a circular 0.3 m^2 Teflon sheet mounted in the chamber. Before starting the irradiation, the chamber was flushed for at least 10 h by 30 L/min of humidified zero air (55–60% RH) in order to provide the humidification of the salt and to get rid of the inherent air intrusion during the insertion of the salt pan. The chemicals used were NaCl ACS (Sigma-Aldrich), $\text{MgCl}_2 \cdot 6\text{H}_2\text{O}$ (VWR), NaBr Suprapur (Merck), $\text{Na}_2\text{SO}_4 \cdot 10\text{H}_2\text{O}$ ACS (Merck), $\text{Na}_2\text{C}_2\text{O}_4$ ACS (Alfa Aesar), $\text{H}_2\text{C}_2\text{O}_4 \cdot 2\text{H}_2\text{O}$ (Merck), $\text{C}_6\text{H}_6\text{O}_2$ (Merck), and $\text{Fe(III)Cl}_3 \cdot 6\text{H}_2\text{O}$ ACS (Sigma-Aldrich).

All in all, a total of 13 salt samples, different in their composition, were investigated under similar conditions, whereas some of them were irradiated twice or up to five times. The pH was determined afterward by adding about 2 g of the salt to 3 mL of bidistilled water in order to obtain a saturated solution and a rough estimate of the pH in the QLM on the salt crystals, especially with respect to relative differences of the salt samples and the thereby induced complex formation. Nonbleeding pH indicator strips (Merck, special indicator pH 0–2.5, 2.5–4.5, and 4.0–7.0) were employed, assuming an uncertainty of ± 0.5 .

2.3. Quantification of Cl, Br, and OH by the Radical Clock Method. Once gaseous Cl_2 , BrCl , and Br_2 molecules were present, they were rapidly photolyzed to atoms by the solar simulator in our setup ($J_{\text{Cl}_2} = 1.55 \times 10^{-3} \text{ s}^{-1}$, $J_{\text{BrCl}} = 7 \times 10^{-3} \text{ s}^{-1}$; $J_{\text{Br}_2} = 1.7 \times 10^{-2} \text{ s}^{-1}$).⁴⁷ To quantify the concentrations of Cl, Br, and OH in the gas phase, the radical clock method^{50,51} was applied after smoothing the observed time profiles of the hydrocarbons⁴⁸ and was extended to bromine atoms when bromide was involved. This was achieved by monitoring the depletion of an inert dilution standard (*n*-perfluorohexane, PFH) and the consumption of selected hydrocarbons (HC_i), namely, 2,2-dimethylpropane (DMP), 2,2-dimethylbutane (DMB), 2,2,4-trimethylpentane (TMP),

Table 1. Salt Compositions, Irradiation Times, Total Initial Reactivity of the HCs in the Chamber against Cl and Br, Cl and Br Concentrations, and the Resulting Minimum and Maximum Cl and Br Sources (neglecting or considering degradation products, respectively), and OH Concentrations

experiment no. ^a	composition (weight [g])	irradiation time [min]	initial Cl/Br reactivity (s ⁻¹)	Cl/Br concentration (10 ⁵ radicals cm ⁻³) ^h	Cl/Br – source Q _X (10 ¹⁰ atoms h ⁻¹ cm ⁻³)	OH concentration (10 ⁶ radicals cm ⁻³) ^h
#1	NaCl (100) ^b	738	114	~5.8	4.1–4.2	~6
#2	NaCl (95), MgCl ₂ ·6H ₂ O (5) ^b	760	62	~9.1	1.9–2.0	~10
#3	NaCl (99.5), NaBr (0.5) ^b	474	60/0.0022	~8.5/~4084	1.6–1.7/2.6–3.1	~4.5
#4	NaCl (98), Na ₂ C ₂ O ₄ (2) ^b	590	44	~1.8	2.7–2.8	~6.2
#5	NaCl (98), C ₆ H ₆ O ₂ (2) ^c	432	41	n.d. ^e	n.d. ^e	~1.8
#6.1	NaCl (98), FeCl ₃ ·6H ₂ O (2) ^c	30	73	~300 ^f	>79–500 ^f	n.d. ^g
#6.2	NaCl (98), FeCl ₃ ·6H ₂ O (2) ^c	341	151	~18	63–89	~6.8
#7.1	NaCl (99.5), FeCl ₃ ·6H ₂ O (0.5) ^c	300	284	~6	52–57	~3.1
#7.2	NaCl (99.5), FeCl ₃ ·6H ₂ O (0.5) ^c	235	231	~390	130–230	~17
#7.3	NaCl (99.5), FeCl ₃ ·6H ₂ O (0.5) ^c	306	195	~2.4	14–15	~1.5
#7.4	NaCl (99.5), FeCl ₃ ·6H ₂ O (0.5) ^c	274	111	~6.2	19–21	~3.5
#7.5	NaCl (99.5), FeCl ₃ ·6H ₂ O (0.5) ^c	165	86	~2.5	7.2–7.6	~4
#8	NaCl (93), FeCl ₃ (2)·6H ₂ O, Na ₂ SO ₄ ·10H ₂ O (5) ^b	311	71	~1.9	5–5.2	~3.5
#9	NaCl (97.5), FeCl ₃ ·6H ₂ O (2), NaBr (0.5) ^b	666	353/0.0088	~1.5/~10195	11–12/27–32	~4.5
#10	NaCl (96), FeCl ₃ ·6H ₂ O (2), Na ₂ C ₂ O ₄ (2) ^d	214	235	~0.8	6.7–6.9	n.d. ^e
#11	NaCl (96), FeCl ₃ ·6H ₂ O (2), C ₆ H ₆ O ₂ (2) ^d	220	297	n.d. ^e	n.d. ^e	~4
#12	NaCl (96), FeCl ₃ ·6H ₂ O (2), H ₂ C ₂ O ₄ ·2H ₂ O (2) ^d	129	85	~5.1	13–15	n.d. ^e
#13	NaCl (91), FeCl ₃ ·6H ₂ O (2), Na ₂ SO ₄ ·10H ₂ O (5), H ₂ C ₂ O ₄ ·2H ₂ O (2) ^c	308	90	~0.5	1.4–1.5	~2.6

^aIn chronological order; two digits indicate multiple irradiations of the same sample. ^bMilled. ^cGround. ^dUntreated. ^eBelow the detection limit. ^fH₂ disappeared within 30 min. ^gCannot be distinguished from Cl. ^hMean over the first hour.

and toluene (Tol), every 15 min by gas chromatography, GC (Siemens Sichromat 2), using an Al₂O₃-PLOT column with 50 m, employing a temperature gradient of 50 °C/min to heat from 160 to 200 °C after 3 min of runtime, using 0.25 mL/min He as the carrier gas, a flame ionization detector (FID), a custom-built liquid nitrogen cryotrap enrichment for focusing the samples with a sampling flow of 100 mL/min for 3 min, and a Nafion dryer. The dilution flow (to maintain the overpressure and replenish the consumption by the gas analytics) was typically 5 L/min, leading to a mean residence time of 12 h of the gas in the chamber. The degradation of the HC_{*i*} in combination with the respective rate constants of their reactions with Cl (*k*_{Cl,*i*}), Br (*k*_{Br,*i*}), and OH (*k*_{OH,*i*}) (Supporting Information, Table S1) allows us to compute time profiles for Cl, Br, and OH by solving the system of *i* differential equations according to eq 1 after fitting an appropriate analytical function to the profile of each HC_{*i*}.

$$-\frac{d[\text{HC}]_i}{dt} = k_{\text{Cl},i}[\text{Cl}][\text{HC}]_i + k_{\text{Br},i}[\text{Br}][\text{HC}]_i + k_{\text{OH},i}[\text{OH}][\text{HC}]_i \quad (1)$$

Dividing by [HC]_{*i*} separates the variables (eq 2) and allows us to identify the contribution of each radical to the consumption of the HC_{*i*} after integration

$$-\frac{d \ln[\text{HC}]_i}{dt} = k_{\text{Cl},i}[\text{Cl}] + k_{\text{Br},i}[\text{Br}] + k_{\text{OH},i}[\text{OH}] \quad (2)$$

Due to the use of four different HC species *i* to determine three unknown variables, the system is overdetermined. The single results are arithmetically averaged, and the standard deviations allow us to obtain a statistical uncertainty of the

result. The steady state of the radicals and atoms, formed by the photochemical processes and consumed by the HCs and their degradation products, delivers concentrations that inversely depend on the initial amount of the HC_{*i*} injected (if wall loss and reactions with CH₄, O₃, and other constituents are neglected), forming a total reactivity of the system toward the respective radical ($\sum_i k_{X,i}[\text{HC}]_i$; X = Cl, Br, or OH). The total production, Q_X, during the time τ can be calculated by equalizing the source and the sinks, assuming a photostationary, steady state ($d[X]/dt = 0$)

$$Q_X = \int_0^\tau \sum_i k_{X,i}[\text{HC}]_{i,t} [X]_t dt \quad (3)$$

Adopting the initial HC concentrations, [HC]_{*i,0*}, and the rate constants of their reactions with the radical X as a constant total reactivity of the chamber contents toward X over the time of the experiment allows us to calculate a maximal value of X. Such an approximation assumes that the reactivity of the reaction products is the same as the reactivity of the HC_{*p*}, which is only valid in the early stage of each experiment at low consumption of the hydrocarbons. By using actually measured, dilution-corrected [HC]_{*i*} values and neglecting any X reactivity of the products, a minimal value of Q_X can be calculated.

3. RESULTS AND DISCUSSION

Salt compositions, treatment, reactivity of the system, resulting Cl and Br sources, and the determined OH concentrations of the 18 performed experiments are listed in Table 1.

3.1. Data Assessment and Evaluation. The development of the gas chromatograms during experiment #6.2 is illustrated in Figure 1.

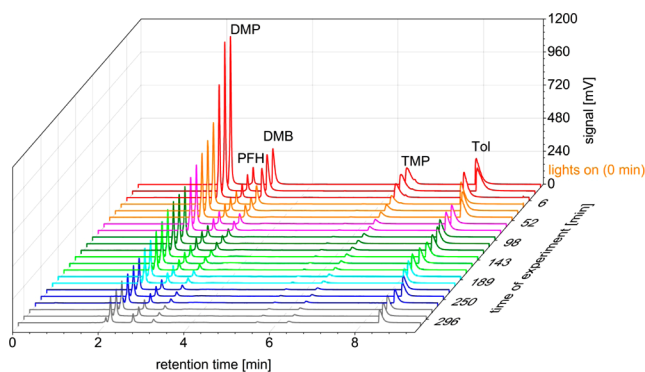


Figure 1. Evolution of the gas chromatograms from experiment #6.2 (2 g of $\text{FeCl}_3 \cdot 6\text{H}_2\text{O}$ /98 g of NaCl), showing the peaks of DMP, PFH, DMB, TMP, Tol, and an unidentified reaction product.

The peaks are manually integrated using the Chemstation software (HPCHEM-Agilent/Rev. B.04.03-SP1). The resulting peak areas of each measurement are corrected for dilution by the signal of the inert standard, PFH, and are shown in Figure 2.

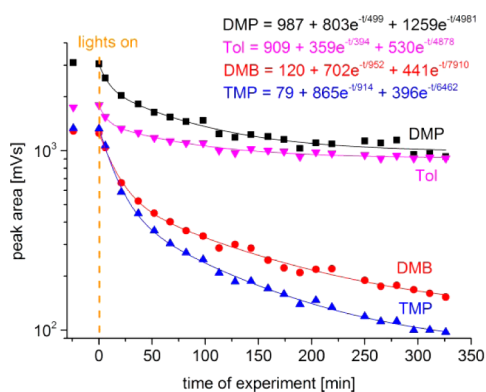


Figure 2. Dilution-corrected time profiles of the integrated HC peak areas from experiment #6.2 (2 g of $\text{FeCl}_3 \cdot 6\text{H}_2\text{O}$ /98 g of NaCl).

The application of the (bi)exponential fit functions displayed in the figure in combination with eq 2 leads to smoothed time profiles for the Cl and OH concentrations (Br is below the detection limit in this experiment) that are shown in Figure 3. Due to the Cl-dominated HC depletion and the low HC reactivity toward OH, the OH evaluation is errorprone and

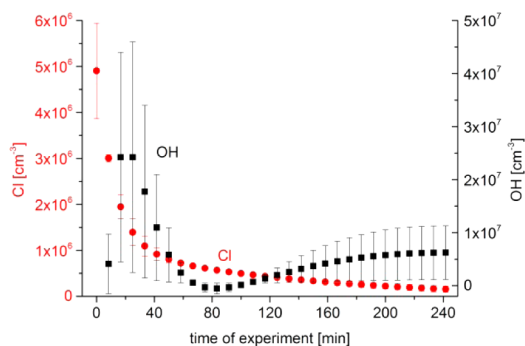


Figure 3. Resulting time profiles for the gaseous Cl and OH concentrations in the 2 g of $\text{FeCl}_3 \cdot 6\text{H}_2\text{O}$ /98 g of NaCl experiment #6.2.

partly shows high uncertainties compared to the result of Cl. Equation 3 allows us to calculate the total source of Cl and OH (and Br if present). This principle was applied for the data evaluation of each experiment and led to the respective results that are discussed in the following sections.

Instead of using (bi)exponential functions, the application of sigmoidal fit functions to the HC_i time profiles may be more appropriate in certain cases. On the other hand, the fit function does not make a difference in the resulting Cl production rates for a large Cl production and an almost immediate depletion of the HC_i . Some experiments instead show a delayed HC_i depletion that results (when applying sigmoidal functions) in an apparent increase of the production rate mainly in the first 30–40 min and a subsequent decrease similar to the (bi)exponential result. These various tendencies in the first 30–40 min (depending on the fit functions) may be considered as an effect of the limited time resolution (3 min cryotrap enrichment and 15 min for each total run) and an inhomogeneous mixing during the sampling time (3–4 min mixing time). However, the resulting total sources (over more than 60 min of the experiment) differ by 20% in extreme cases at most.

For typical $[\text{HC}]_i$ concentrations of 10 ppb ($\sim 2.5 \times 10^{11}$ molecules cm^{-3}), the approximate detection limit of the method for the radical concentrations is for Cl atoms 10^4 molecules cm^{-3} , for Br atoms 10^9 molecules cm^{-3} , and for OH 10^6 molecules cm^{-3} , leading to detectable production rates, dQ_x/dt , of about 10^6 molecules $\text{cm}^{-3} \text{s}^{-1}$ for Cl, 10^8 molecules $\text{cm}^{-3} \text{s}^{-1}$ for OH, and 10^{11} molecules $\text{cm}^{-3} \text{s}^{-1}$ for Br, depending on the various reactivities of the HCs that differ in this range. For example, when Cl is present at significant levels, a 3 orders of magnitude higher Br concentration is needed to detect a contribution to the depletion of the HC_i . The detection limit and its uncertainty are characterized, for example, by the duration of the cold trap enrichment (currently 3 min) that limits the time resolution, by various wall loss rates compared to PFH, and by the fit functions that are applied to the profiles of each HC_i .

Alternatively to the evaluation method described above (when Br is not involved), one may integrate eq 2 and divide it by k_{OH} to solve the system graphically by exponential fits of the HC data for each measurement⁵¹

$$-\ln([\text{HC}_i(\tau)]/[\text{HC}]_{i,0})/k_{\text{OH},i} = k_{\text{Cl},i}/k_{\text{OH},i} \int_0^\tau [\text{Cl}] dt + \int_0^\tau [\text{OH}] dt \quad (4)$$

This leads directly to time-integrated Cl and OH concentrations that are responsible for the measured HC depletion for each time of the sampling, whereas the initial fits of the HC_i profiles lead to smoothed results for $\int [\text{Cl}] dt$ and $\int [\text{OH}] dt$.

Figure 4 compares the two evaluation methods based on experiment #6.2, where the resulting concentrations of the HC fit were integrated over time and plotted against the directly obtained, time-integrated results of the linear regression method. The absolute values and the time profiles are in very good agreement, except for the varying uncertainties that are caused by the statistical uncertainty of the combination of six Cl and OH results, each obtained by two HCs on the one hand and the standard error of one linear regression on the other hand.

3.2. Blank Experiments with Iron-Free Salt Pans. In order to investigate the effects of Fe(III) enrichment in a salt

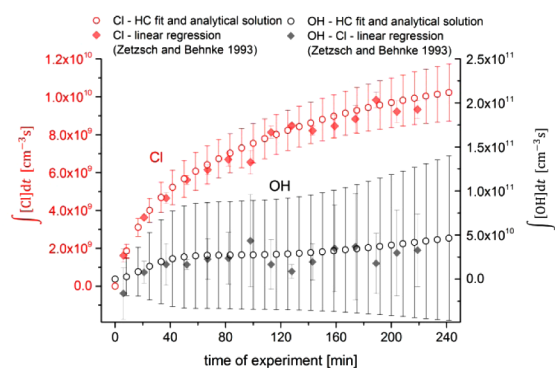


Figure 4. Time-integrated quasi-stationary Cl and OH concentrations derived from experiment #6.2 by the biexponential HC fit method described in section 2.3 (circles) in comparison to the evaluation proposed by Zetzsch and Behnke (diamonds).⁵¹

sample, blank experiments were conducted by using iron-free salts. Except for the catechol sample, all blank samples were milled and thus featured a finer grain size and a larger specific surface as compared to the ground and untreated samples.

Figure 5a and b presents the Cl and Br production rates (dQ_X/dt) and the corresponding Cl and Br sources (Q_X) resulting from the blank experiments with pure NaCl (experiment #1) and with added NaBr (experiment #3). The graphs start where the irradiation of the sample was started ($t = 0$ min). The lower and upper margins of the bars represent the minimal and maximal values of dQ_X/dt and Q_X , as described in section 2.3. The negative minimal and maximal uncertainties are drawn as thinner error bars for dQ_X/dt . Most measurements for Cl and Br from the blank samples are close to the detection limit and therefore show a large uncertainty. Further blank measurements include magnesium chloride, sodium oxalate, and catechol (experiments #2, #4, #5) and are shown in the Supporting Information.

For the pure NaCl sample, a source of atomic Cl of $(4.1\text{--}4.2) \times 10^{10} \text{ cm}^{-3}$ was detected for the first hour, corresponding to production rates of $(0.8\text{--}1.5) \times 10^7 \text{ cm}^{-3} \text{ s}^{-1}$ (see Figure 5a or Table 1). Excluding the Fe(III)-induced chloride and bromide activation, this Cl_2 release can possibly be attributed to bromide impurities in the salt ($\text{Br}^-: \leq 0.01\%$, according to the specifications of the manufacturer Sigma-Aldrich S9888, $\geq 99.0\%$) and to the observed NO_X impurities contained in the zero air and introduced due to the inherent air intrusion

during the opening of the chamber required to change the salt samples. For such high Cl/Br ratios, bromide mainly induces the activation of chloride by the formation of BrCl^{16} that is released into the gas phase and rapidly photolyzed in our system ($J_{\text{BrCl}} = 7 \times 10^{-3} \text{ s}^{-1}$). The simultaneously produced Br atoms are below the detection limit due to the low reactivity of the HC_i toward Br. Assuming the release of Br atoms to be comparable with the detected Cl source and combining this assumption with the effect of bromide enrichment on the crystal surface,⁵² a trace impurity of 0.01% may be sufficient to be responsible for the detected Cl atoms.

Furthermore, there is the possibility of a direct activation by the heterogeneous reaction of NO_X trace impurities with the solid salt to subsequently release ClNO ,⁵³ which could be photolyzed in our system to form Cl atoms ($J_{\text{ClNO}} = 1.8 \times 10^{-3} \text{ s}^{-1}$) or be hydrolyzed to form HCl and HONO and thus induce an enhanced OH production.⁵⁴ In the presence of O_3 (leading to N_2O_5 from NO_X), ClNO_2 could be formed⁵³ that is more stable against hydrolysis¹⁸ and can be photolyzed to form Cl and NO_2 ($J_{\text{ClNO}_2} = 2 \times 10^{-4} \text{ s}^{-1}$). This summarizes the activation of Cl via uptake of, for example, NO_2 , N_2O_5 , and O_3 on the deliquesced salt, and concomitant release of photolyzable precursors.^{38,53} Throughout the experiments, typical O_3 and NO_X concentrations remained below 15 ppb ($\sim 3.8 \times 10^{11} \text{ molecules cm}^{-3}$) and 2 ppb ($\sim 5 \times 10^{10} \text{ molecules cm}^{-3}$), respectively, whereas a slight O_3 formation was observed in the course of the irradiation.

The resulting OH concentrations mainly ranged between 10^6 and $10^7 \text{ molecules cm}^{-3}$, as shown in Table 1. In our system, gaseous OH is mainly produced by NO_X impurities in the zero air. The ongoing well-known photochemical cycle produces nitrogen monoxide, which may reduce HO_2 radicals, which originate from the oxidation of hydrocarbons. Furthermore, NO can form O_3 via RO_2 and finally OH from photolysis of O_3 in the presence of water vapor. The known storage of NO_X in the FEP film and release under UV irradiation, mainly in the form of HONO,⁵⁵ can also form OH ($J_{\text{HONO}} = 1.5 \times 10^{-3} \text{ s}^{-1}$).

The contribution of the CH_4 impurity in the zero air (50–100 ppb) and of the O_3 formation during the experiment to the total Cl and OH reactivity in the system is lower than 5% for both radicals during the entire experiment and therefore neglected in the evaluation. Concerning Br, the reactivity of O_3 (formed during the experiments) can possibly influence the evaluation of the production rates and sources with respect to the low HC reaction rates toward Br. However, the Br-induced

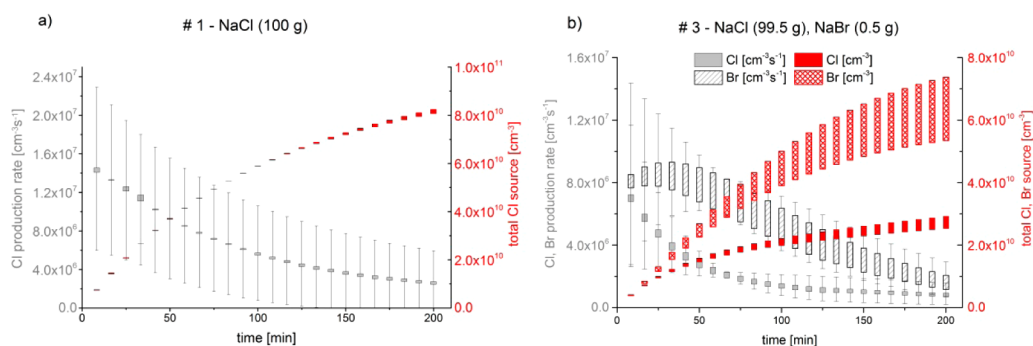


Figure 5. (a,b) Production rates of Cl and Br [$\text{atoms cm}^{-3} \text{ s}^{-1}$] and the integrated total Cl and Br source [atoms cm^{-3}] during the blank experiments #1 and #3 (corresponding figures for the experiments #2 and #4 are shown in the Supporting Information). The salt compositions are given in the figures. The lower and upper margins of the bars represent the minimal and maximal values. For the production rate, the negative minimum and the positive maximum uncertainties are included as thin error bars.

Table 2. Rate Constants for Reactions and Equilibria Involving Cl^\bullet , $\text{ClOH}^{\bullet-}$, $\text{Cl}_2^{\bullet-}$, and OH^\bullet Radicals (given for zero ionic strengths)

reaction	k_+ (forward) ($\text{M}^{-1} \text{s}^{-1}$)	k_- (backward) (s^{-1})	no.
$\text{OH}^\bullet + \text{Cl}^- \rightleftharpoons \text{ClOH}^{\bullet-}$	4.2×10^9	6.0×10^9	R5 ⁶⁴
$\text{ClOH}^{\bullet-} + \text{H}^+ \rightleftharpoons \text{Cl}^\bullet + \text{H}_2\text{O}$	2.4×10^{10}	1.8×10^5	R6 ⁶⁴
$\text{Cl}^\bullet + \text{Cl}^- \rightleftharpoons \text{Cl}_2^{\bullet-}$	7.8×10^9	5.7×10^4	R7 ⁶⁴
$\text{Cl}^\bullet + \text{Cl}_2^{\bullet-} \rightleftharpoons \text{Cl}^- + \text{Cl}_2$	1.4×10^9		R8 ⁶⁴
$\text{Cl}_2^{\bullet-} + \text{Cl}_2^{\bullet-} \rightarrow \text{Cl}_3^- + \text{Cl}^-$	3.1×10^9		R9 ⁶⁵
$\text{Cl}_3^- \rightleftharpoons \text{Cl}_2 + \text{Cl}^-$	$K = 1.8 \times 10^{-1} \text{ M}^{-1}$		R10 ⁶⁶
$\text{Cl}^\bullet + \text{Fe}^{2+} \rightarrow \text{Cl}^- + \text{Fe}^{3+}$	5.9×10^9		R11 ⁶⁷
$\text{Cl}_2^{\bullet-} + \text{Fe}^{2+} \rightarrow 2\text{Cl}^- + \text{Fe}^{3+}$	1.4×10^7		R12 ⁶⁸
$\text{ClOH}^{\bullet-} + \text{Fe}^{2+} \rightarrow \text{Cl}^- + \text{OH}^- + \text{Fe}^{3+}$	1.3×10^8		R13 ⁶⁷
$\text{OH}^\bullet + \text{Fe}^{2+} \rightarrow \text{OH}^- + \text{Fe}^{3+}$	2.7×10^8		R14 ⁶⁹
$\text{OH}^\bullet + \text{OH}^\bullet \rightarrow \text{H}_2\text{O}_2$	5.2×10^9		R15 ⁶⁹

O_3 destruction recycles Br via BrO and HOBr and thus does not represent a final sink. At least during the first hour of the experiments, where the HC and O_3 reactivities are comparable and O_3 starts to form, the resulting Br concentrations are significant.

All experiments show a general trend to lower production rates with progressing irradiation time. A simple explanation for this tendency could be the evaporation of water from the QLM on the salt due to the radiative heating of the salt pan by the solar simulator, thus diminishing the mobility of the halide ions. This may cause a surface “passivation” when the available halide ions have been consumed.³⁸

Despite the hygroscopic properties of MgCl_2 and the possibly more pronounced QLM,⁵⁶ a comparison of the Cl yields from the NaCl sample with the MgCl_2 sample shows a lower Cl_2 release. Also, the addition of 2 g of sodium oxalate led to lower Cl activation with respect to pure NaCl. Catechol (that is very soluble and acts as a reducing agent) strongly inhibits the Cl_2 formation and shows a Cl production rate below the detection limit. Except for toluene, the depletion of the injected HC mixture was hardly observable; thus, the resulting Cl production rate and total Cl source could not be detected because no suitable fit function could be found for the alkanes.

The effect of bromide on a NaCl sample was observed by adding 0.5 g of NaBr to 99.5 g of NaCl. A Br source of $(2.6\text{--}3.1) \times 10^{10} \text{ cm}^{-3}$ was detected in the first hour, whereas the Cl source did not show a marked difference to the pure NaCl salt. During crystallization, bromide was enriched on the surface with respect to chloride;⁵² thus, the molar Cl/Br ratio and the resulting ratio in the QLM will probably be lower than the measured ratio in the saturated liquid phase (Cl/Br = 150) where much more water was used (section 3.4). Additionally, the activation mechanisms favor the production of Br_2 instead of BrCl at these Cl/Br ratios,¹⁶ explaining the high Br source (Figure 5b). For example, Hirokawa et al.⁵⁷ and Mochida et al.⁵⁸ found that the heterogeneous Br_2 formation through the uptake of O_3 on sea salt is much more effective, whereas a Cl_2 release was not observed in these studies. Oum et al.⁵⁹ proposed that gas-phase OH radicals can heterogeneously produce Cl_2 and Br_2 from sea salt.^{56,60,61} The uptake of OH on salt solutions and subsequent release of Br_2 , BrCl, and Br_2 have been investigated by Frinak and Abbatt,⁶² Park et al.,^{56,60,61} and

Nissenson et al.⁶³ in detail. As O_3 ($10\text{--}20 \text{ ppb}$, $2.5\text{--}5 \times 10^{11} \text{ molecules cm}^{-3}$) and OH radicals ($10^6\text{--}10^7 \text{ molecules cm}^{-3}$) are formed during irradiation in our experiments, these mechanisms would explain the observed Cl and Br sources.

On the basis of the steady-state concentrations of atomic Cl measured by Buxmann et al.⁴⁷ above a 0.33 g of NaBr and 100 g of NaCl salt mixture, one can calculate Cl production rates of $(1.3\text{--}1.8) \times 10^7 \text{ cm}^{-3} \text{ s}^{-1}$ for the experiments with 200 ppb ozone at 67% RH. In comparison, our production rates vary from $(0.4\text{--}1.7) \times 10^7 \text{ cm}^{-3} \text{ s}^{-1}$. The given BrO production rates of 10–30 ppt/s (and thus the Br production), corresponding to $(2\text{--}7) \times 10^8 \text{ BrO atoms cm}^{-3} \text{ s}^{-1}$ at standard conditions, seem to be much higher in the work by Buxmann et al.⁴⁷ than that in our study, where $(2\text{--}8) \times 10^6 \text{ Br atoms cm}^{-3} \text{ s}^{-1}$ were detected in experiment #3. However, these results are difficult to compare due to the high ozone concentrations, the lower NaBr content, and the higher RH.

3.3. $\text{FeCl}_3 \cdot 6\text{H}_2\text{O}$ -Containing Salts. Once dissolved in the aqueous phase, Fe(III) forms light-absorbing complexes with available ions and water molecules. The speciation mainly depends on salt composition, pH, and ionic strength in the solution and has a significant influence on the photoinduced radical formation. In the Fe(III)/water system, the main complexes are $\text{Fe}(\text{H}_2\text{O})_6^{3+}$ and $\text{Fe}(\text{H}_2\text{O})_5\text{OH}^{2+}$ at low pH, whereas in the presence of chloride anions, the more photosensitive $\text{Fe}(\text{H}_2\text{O})_5\text{Cl}^{2+}$ and $\text{Fe}(\text{H}_2\text{O})_4\text{Cl}_2^+$ complexes become important.^{33,36} For convenience, coordinated water molecules $(\text{H}_2\text{O})_x$ will be omitted in the following. Photolysis of these complexes leads to OH and Cl radicals according to reactions R1–R4.

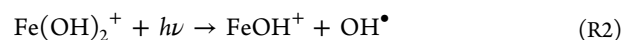


Table 2 summarizes the main reaction pathways in chloride-dominated media and their forward (k_+) and backward (k_-) reaction rate constants. In the preponderant presence of chloride, OH^\bullet and Cl^\bullet will predominantly be scavenged by Cl^- to form the intermediates $\text{ClOH}^{\bullet-}$ and $\text{Cl}_2^{\bullet-}$, respectively (Table 2, equilibria R5 and R7). Depending on the pH,

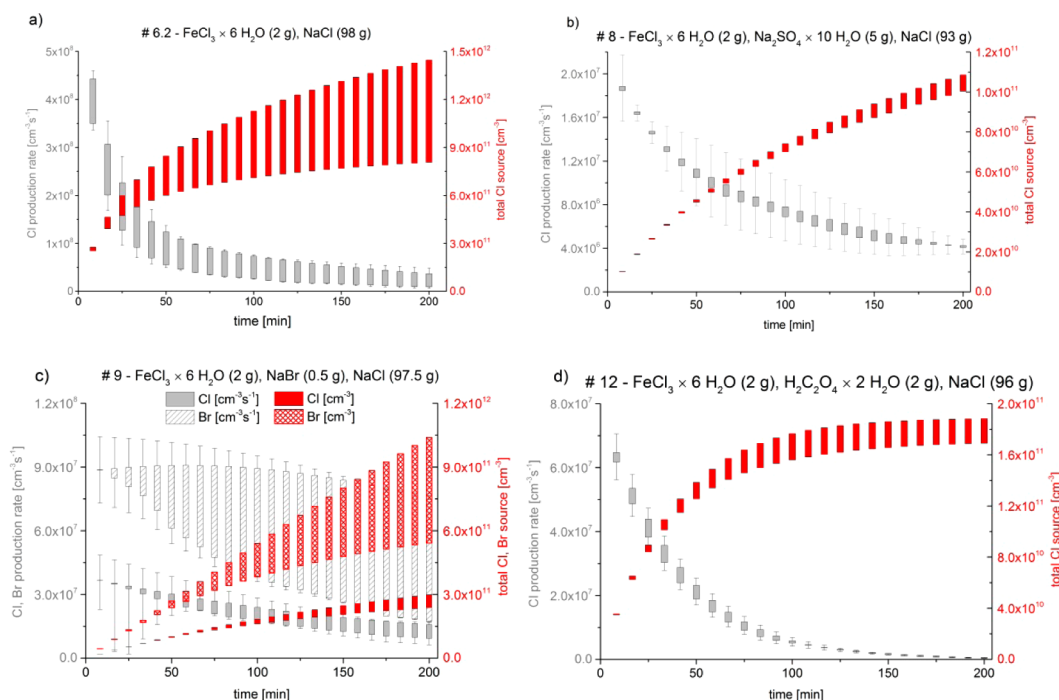


Figure 6. (a–d) Production rates of Br and Cl [atoms cm⁻³ s⁻¹] and the integrated total source of Cl and Br [atoms cm⁻³] during the FeCl₃·6H₂O experiments #6.2 (a), #8 (b), #9 (c), and #12 (d) (corresponding figures for the experiments #7.1, #10, and #13 are shown in the Supporting Information). The lower and upper margins of the bars represent the minimal and maximal values. For the production rate, the negative minimum and the positive maximum uncertainties are included as thin error bars.

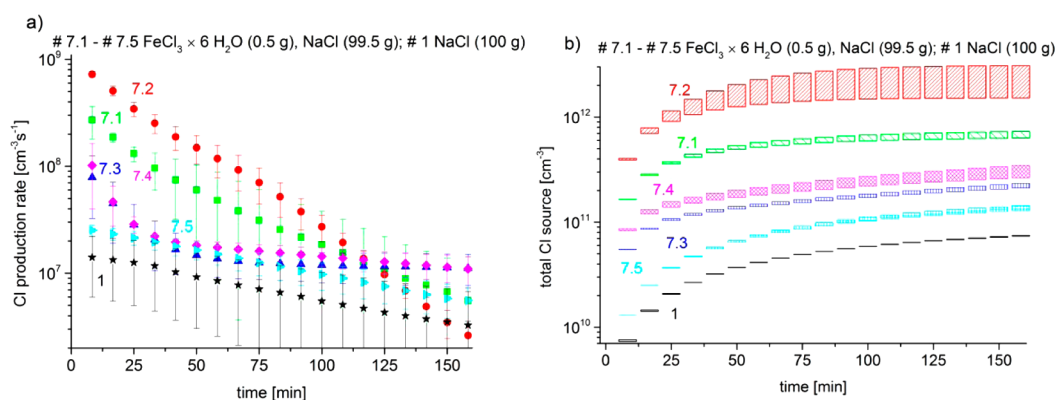


Figure 7. (a,b) Cl production rates [atoms cm⁻³ s⁻¹] detected in the repetitive irradiation of the 0.5 g of FeCl₃·6H₂O/99.5 g of NaCl sample (experiments #7.1–#7.5) in comparison with the blank run on pure NaCl (experiment #1) (a) and the resulting total Cl source [atoms cm⁻³] for the same experiments (b).

ClOH^{•-} can dissociate to Cl[•] (Table 2, equilibrium R6) that again produces Cl₂^{•-}. Thus, the photolysis of FeOH²⁺ and Fe(OH)₂⁺, primarily producing OH[•], finally forms Cl₂^{•-},⁷⁰ which is able to degas according to its physical solubility (Henry's law constant at 298 K: 6.2–9.5 × 10⁻² M atm⁻¹).⁷¹ However, the photolysis reactions R3 and R4, which directly produce Cl[•] and finally lead to a degassing of Cl₂, are much more effective based on the absorption cross sections and quantum yields.^{72,73} The degassing of Cl₂ slows down with increasing pH when the hydrolysis to the poorly degassing hypochlorous acid (ClOH) is favored between pH 4 and 7 (Henry's law constant at 298 K: 2.6–9.3 × 10² M atm⁻¹).⁷¹ The high concentration of Cl⁻ and the subsequent scavenging of the radical intermediates Cl[•] and OH[•] (R5 and R7, Table 2) will outmatch the reactions R11, R14, and R15 (Table 2), involving Fe²⁺ and H₂O₂.⁷⁰ Solely,

Fe²⁺ may become a sink for Cl₂^{•-} with advanced photolytic reduction of Fe³⁺ after long irradiation times.

In comparison to the blanks, the addition of FeCl₃·6H₂O generally led to an increase in the observed gaseous Cl except for samples where sulfate was involved. The production rate showed a downward trend similar to that of the blank experiments. The reason is not only the drying out of the sample but also the formation of iron(II) via photoreduction (reactions R1 and R3) that becomes a sink for the radical intermediates Cl[•], ClOH[•], and OH[•] or even directly reacts with Cl₂^{•-} (Table 2, reactions R11–R14), inhibiting the further formation of Cl₂.³⁷ However, the reactions with Cl⁻ (Table 2, reactions R5 and R7) will dominate because Cl⁻ in the QLM is constantly provided by the bulk sample and the concentration is not expected to change significantly during irradiation.

The 2 g of $\text{FeCl}_3 \cdot 6\text{H}_2\text{O}$ /98 g of NaCl salt pan (experiment #6.1) showed an enormous Cl_2 release and consumed all of the injected alkanes totally within the first 30 min of irradiation.

Due to the restricted time resolution with only two measuring points, the Cl source can only be estimated. The injected amount of HCs was increased for the next experiments. In experiment #6.2, the same sample as that in #6.1 was used, resulting in an up to 30 times higher production rate of Cl with respect to a pure 100 g of NaCl salt pan (see Figures 5a and 6a) without considering the additional effect of the probably smaller specific surface of the ground $\text{FeCl}_3 \cdot 6\text{H}_2\text{O}$ -containing samples and the reuse of the sample that had already been exposed to the simulated sunlight for 30 min. The total Cl source in the chamber increased up to $(6.3\text{--}8.9) \times 10^{11}$ atoms cm^{-3} during 60 min of irradiation. Assuming that (without recycling) each Fe(III) species produces one Cl atom that leads to a degassing of $(1/2)\text{Cl}_2$ molecule, at least a portion of 0.05–0.07% of the added Fe(III) is involved in the photoproduction of Cl_2 . A reduction of the FeCl_3 hexahydrate fraction in the salt from 2 to 0.5 g in 99.5 g of NaCl (experiment #7.1) led to a slight decrease in the production rate and the total Cl source of only $(5.2\text{--}5.7) \times 10^{11}$ atoms cm^{-3} during the first 60 min (see Figure 7a,b or Figure S2a in the Supporting Information). The enhanced activation can be attributed to the iron-induced chlorine release mechanism as described above. Furthermore, the drop in pH due to the $\text{FeCl}_3 \cdot 6\text{H}_2\text{O}$ addition causes a shift in the speciation and supports the formation of the photosensitive FeCl_2^+ and FeCl^{2+} complexes as well as the degassing of Cl_2 (see section 3.4).

To investigate possible regeneration effects and check if the Cl source can become exhausted, experiment #7.1 was repeated five times without a change of the sample after dark periods of 1 night for experiments #7.1–7.3, of 1 week between #7.3 and #7.4, and of 3 nights between #7.4 and #7.5 without irradiation. A systematic tendency toward a lower Cl activation or an increased source after longer regeneration times are hardly noticeable (Figure 7a,b). Rather significant is the systematically higher Cl production rate ($10^7\text{--}10^9$ $\text{cm}^{-3} \text{ s}^{-1}$) and thus the elevated Cl source in each run in comparison with the pure NaCl sample ($0.8\text{--}1.5 \times 10^7$ $\text{cm}^{-3} \text{ s}^{-1}$). Each resulting Cl source was at least above 10^{11} cm^{-3} after 100 min compared to $(5.8\text{--}5.9) \times 10^{10}$ cm^{-3} for the blank experiment with 100 g of NaCl.

The addition of sodium sulfate and catechol to the 2 g of $\text{FeCl}_3 \cdot 6\text{H}_2\text{O}$ /98 g of NaCl mixture hindered the chloride activation drastically (Table 1 or Figure 6b). In both cases, the color of the sample changed to yellow and black, respectively, indicating a complex formation during the sample production process because sodium sulfate and catechol are usually colorless, although it does not seem to be in agreement with the speciation in chloride-dominated media (section 3.4). The observed yellow salt complexes in the sulfate sample are able to reduce the light intensity in the spectral region that is important for the photolysis of the Fe(III)–Cl complexes. The produced ferrous ions in reactions R1 and R3 prefer to form the stable FeSO_4 complex with the available sulfate ions ($\log K = 1.35$)⁷⁴ and thus interrupt the regeneration of Fe^{2+} to Fe^{3+} . Furthermore, SO_4^{2-} and HSO_4^- ions can act as scavenger for Cl^\bullet and OH^\bullet , producing sulfate anion radicals, and inhibit the formation of Cl_2 .³⁴ Thus, sulfate is able to strongly inhibit the radical production and Cl_2 release, as is observed in experiment #8 (Figure 6b). The Cl source is quantified to be even lower than that of the pure NaCl sample despite the same treatment

(both milled). The inhibiting effect of catechol is even more intense and led to a Cl production rate below the detection limit, as compared to the blank experiment where only catechol (2 g) and NaCl (98 g) were present. Here, the well-known rapid redox reduction of Fe(III) to Fe(II) may play a decisive role, oxidizing catechol via quinone to muconic acid and finally in a few hours to CO_2 .⁷⁵

Two effects were observed for the $\text{Na}_2\text{C}_2\text{O}_4$ (2 g)/ $\text{FeCl}_3 \cdot 6\text{H}_2\text{O}$ (2 g)/NaCl(98 g) mixture. As discussed in section 3.4, oxalate forms a stable and dominant complex with Fe(III) that diminishes the Fe(III)–Cl complexation and thus the direct activation of chloride. Moreover, sodium oxalate shifts the sample pH to a less acidic range, where FeCl_2^+ starts to be reduced and the Cl_2 release is restricted by the formation of hypochlorous acid. Experiment #12 (Figure 6d) demonstrates the sensitivity to the pH by the use of oxalic acid instead of sodium oxalate, resulting in a more acidic pH of about 5. Due to this change, the Cl source in the first 60 min slightly increased from $(6.7\text{--}6.9) \times 10^{10}$ to $(13\text{--}15) \times 10^{11}$ cm^{-3} . According to Zuo and Hoigné,⁷⁶ the photolysis of the Fe(III)–oxalate complexes leads to a formation of H_2O_2 and thus stimulates the photo-Fenton reaction and the subsequent reoxidation of Fe(II). The thereby induced Fe(III) recycling and regeneration of photosensitive Fe(III) chloride and hydroxy complexes explains the quite constant Cl production rate at later stages of the experiments when oxalate is involved. However, the high fraction of oxalate in the sample reduces the Fe(III) involved in the photoinduced Cl^\bullet production and thus reduces the total gaseous Cl source.

Experiment #13 demonstrates a combination of the effects from 2 g of oxalic acid and 5 g of sulfate on the 2 g of $\text{FeCl}_3 \cdot 6\text{H}_2\text{O}$ /91 g of NaCl sample. Though the sample was ground, a much lower Cl source of $(1.4\text{--}1.5) \times 10^{10}$ cm^{-3} was observed in the first hour compared to the untreated oxalic acid sample. The lower Cl production in comparison with the milled sulfate sample (experiment #8) can be ascribed to the larger grain size of the ground sample in experiment #13 and the combination of the radical scavenging effect of sulfate and the complexation of oxalate with Fe(III).

The influence of NaBr on the iron-induced chloride activation is similar to the effect on pure NaCl as a lower Cl production was observed in comparison with the respective sample without bromide (Figure 6c). The Br source in the presence of Fe(III) was a factor of 12 higher than that in the absence of Fe(III) in the first hour (Table 1), whereas the Cl source was 6–8 times lower due to the bromide addition. This implies that dissolved Fe(III) leads to a stronger preference of bromide activation even if Fe(III) prefers to complex with chloride (section 3.4). However, the photochemically formed Cl_2 seems not to degas completely but rather oxidize bromide to Br_2 as, for example, proposed by Mochida et al.⁷⁷ Furthermore, comparable to the blank sample, an enrichment of bromide on the surface and thus in the aqueous phase on the salt crystals is probable, and the activation of bromide and autocatalytic release of Br_2 instead of BrCl is preferred at this pH and Br^-/Cl^- ratio of 0.0067 in the liquid phase.¹⁶ In fact, Sadanaga et al.⁷⁸ reported an enhancement of the O_3 uptake and Br_2 release in the presence of Fe^{3+} in synthetic sea salt and suggested a Cl_2 release when bromide becomes deficient.

3.4. Speciation. The decisive factor for the photoinduced chlorine release is the fraction of photosensitive iron complexes in the water–chloride system, depending on the pH, molar fractions, and ionic strength. Table 3 gives an overview on the

Table 3. Equilibrium Constants ($\log_{10} K$) for the Formation of Low Molecular Weight Fe(III) Complexes with Several Ligands (including their dissociation constants) at Zero Ionic Strength and 298 K

equilibrium	$\log_{10} K$	no.
Water		
$\text{Fe}^{3+} + \text{H}_2\text{O} \rightleftharpoons \text{FeOH}^{2+} + \text{H}^+$	-2.19	R16 ⁷⁹
$\text{Fe}^{3+} + 2\text{H}_2\text{O} \rightleftharpoons \text{Fe}(\text{OH})_2^+ + 2\text{H}^+$	-5.67	R17 ⁷⁹
$\text{Fe}^{3+} + 3\text{H}_2\text{O} \rightleftharpoons \text{Fe}(\text{OH})_3 + 3\text{H}^+$	-12.0	R18 ⁷⁹
$\text{Fe}^{3+} + 4\text{H}_2\text{O} \rightleftharpoons \text{Fe}(\text{OH})_4^- + 4\text{H}^+$	-21.6	R19 ⁷⁹
Chloride		
$\text{Fe}^{3+} + \text{Cl}^- \rightleftharpoons \text{FeCl}^{2+}$	1.48	R20 ⁸⁰
$\text{Fe}^{3+} + 2\text{Cl}^- \rightleftharpoons \text{FeCl}_2^+$	2.13	R21 ⁸¹
$\text{Fe}^{3+} + 3\text{Cl}^- \rightleftharpoons \text{FeCl}_3$	1.13	R22 ⁸²
Bromide		
$\text{Fe}^{3+} + \text{Br}^- \rightleftharpoons \text{FeBr}^{2+}$	0.61	R23 ⁸³
$\text{Fe}^{3+} + 2\text{Br}^- \rightleftharpoons \text{FeBr}_2^+$	0.2	R24 ⁸³
Sulfate		
$\text{SO}_4^{2-} + \text{H}^+ \rightleftharpoons \text{HSO}_4^-$	1.99	R25 ⁶⁹
$\text{Fe}^{3+} + \text{SO}_4^{2-} \rightleftharpoons \text{FeSO}_4^+$	3.92	R26 ⁶⁹
$\text{Fe}^{3+} + 2\text{SO}_4^{2-} \rightleftharpoons \text{Fe}(\text{SO}_4)_2^-$	5.42	R27 ⁶⁹
Oxalate		
$\text{C}_2\text{O}_4^{2-} + \text{H}^+ \rightleftharpoons \text{HC}_2\text{O}_4^-$	4.18	R28 ⁸¹
$\text{HC}_2\text{O}_4^{2-} + \text{H}^+ \rightleftharpoons \text{H}_2\text{C}_2\text{O}_4$	1.31	R29 ⁴¹
$\text{Fe}^{3+} + \text{C}_2\text{O}_4^{2-} \rightleftharpoons \text{Fe}(\text{C}_2\text{O}_4)^+$	8.77	R30 ⁸¹
$\text{Fe}(\text{C}_2\text{O}_4)^+ + \text{C}_2\text{O}_4^{2-} \rightleftharpoons \text{Fe}(\text{C}_2\text{O}_4)_2^-$	6.52	R31 ⁸¹
$\text{Fe}(\text{C}_2\text{O}_4)_2^- + \text{C}_2\text{O}_4^{2-} \rightleftharpoons \text{Fe}(\text{C}_2\text{O}_4)_3^{3-}$	4.44	R32 ⁸¹
Catechol		
$\text{C}_6\text{H}_6\text{O}_2^{2-} + \text{H}^+ \rightleftharpoons \text{HC}_6\text{H}_6\text{O}_2^-$	13	R33 ⁸⁴
$\text{HC}_6\text{H}_6\text{O}_2^- + \text{H}^+ \rightleftharpoons \text{H}_2\text{C}_6\text{H}_6\text{O}_2$	9.25	R34 ⁸⁴
$\text{Fe}^{3+} + \text{H}_2\text{C}_6\text{H}_6\text{O}_2 \rightleftharpoons \text{Fe}(\text{C}_6\text{H}_6\text{O}_2)^+ + 2\text{H}^+$	1.37	R35 ⁴²
$\text{Fe}^{3+} + \text{C}_6\text{H}_6\text{O}_2^{2-} \rightleftharpoons \text{Fe}(\text{C}_6\text{H}_6\text{O}_2)^+$	20	R36 ⁸⁴
$\text{Fe}(\text{C}_6\text{H}_6\text{O}_2)^+ + \text{C}_6\text{H}_6\text{O}_2^{2-} \rightleftharpoons \text{Fe}(\text{C}_6\text{H}_6\text{O}_2)_2^-$	14.7	R37 ⁸⁴
$\text{Fe}(\text{C}_6\text{H}_6\text{O}_2)_2^- + \text{C}_6\text{H}_6\text{O}_2^{2-} \rightleftharpoons \text{Fe}(\text{C}_6\text{H}_6\text{O}_2)_3^{3-}$	9.01	R38 ⁸⁴

complexes and their equilibrium constants. On the basis of this data, the software PHREEQC⁸⁵ was employed for aqueous, geochemical calculations to derive the speciation as a function of pH in the QLM. To approximate the experimental conditions, small salt samples with equal molar ratios of the components were prepared in small Petri dishes, and 10 mL of bidistilled water was added to obtain a saturated liquid layer on the salt crust. Using a pipet, 1 mL of the liquid phase was taken and diluted 1:10000 in order to analyze for the molar concentrations of iron and present anions by ICP-MS and IC. In this way, the molar ratios of the elements were determined and used as starting parameters for the speciation model. This approach is rather qualitative because the process of adding water differs from the process of humidification by air moisture. The excess of water penetrates through the surface of the salt crystal and allows the bulk to dissolve, whereas the QLM on the crystals is only formed on the surface. Therefore,

the obtained molar ratios could differ from the ratios in the bulk since, for example, bromide is enriched on the surface with respect to chloride during the drying process.⁵² A further consequence of the partly heterogeneous crystallization of the salts is the variation of the liquid film thickness, depending on the hygroscopicity and composition of the different micro-crystalline fractions of the salt pan.

The equilibrium model in PREEQC is based on the MINTEQC database⁸⁶ and was extended for oxalate and catechol including the equilibrium constants listed in Table 3. For Fe^{3+} , Na^+ , Cl^- , SO_4^{2-} , HSO_4^- , and Br^- , the activity coefficients were corrected for the ionic strength based on Pitzer's ion interaction approach⁸⁷ and the respective binary and ternary parameters listed in Tosca et al.⁸⁸ For the other ions, where to date no Pitzer parameters are available, the extended (or WATEQ) Debye-Hueckel equation was applied.^{89,90} The significance of this basic approach involves a large uncertainty because the extended Debye-Hueckel equation is limited to ionic strengths below 1 mol/L but, in the case of predominant Cl^- concentrations, still in good agreement with the Pitzer equations^{91,92} that are able to predict the activity coefficients in solutions with very high ionic strengths.⁹³ The modeled speciation only describes the equilibrium condition at the beginning of each experiment but is able to explain the precondition of the mechanism responsible for the various pathways of Cl_2 production. Detailed model studies, including reaction kinetics and absorptivities, have been performed elsewhere at lower Cl^- levels.^{35,44,69}

Figure 8a and b displays the calculated speciation equilibria for selected samples as a function of pH. The formed Fe(III) complexes are plotted as molar fraction of total Fe(III) dissolved in the QLM on the sample. Due to the high $\text{Cl}^-/\text{Fe}(\text{III})$ ratio, no difference in speciation can be seen for the samples with 2 and 0.5 g of $\text{FeCl}_3 \cdot 6\text{H}_2\text{O}$ except for the absolute concentrations that are shifted. In the expected very acidic pH range of the sample, FeCl_2^+ and FeCl^{2+} represent the highest fraction of Fe(III) species. These species have a much higher absorbance than the Fe(III)-hydroxo complexes.^{36,73} In particular, FeCl^{2+} has a two times higher quantum yield for photodissociation than FeOH^{2+} .³³ An even higher molar absorptivity in the visible region have Fe(III)-bromine complexes. In the case of FeBr_2^+ , this was shown by Rabinowitch and Stockmayer.⁹⁴ However, our model calculations show a negligible formation of Fe-Br complexes with respect to an assumed Cl^-/Br^- ratio of 150 in the quasi-liquid phase (see Figure S4b in the Supporting Information).

Adding sulfate to the modeled solutions does not significantly change the speciation at low pH on the condition that the molar $\text{Cl}^-/\text{SO}_4^{2-}$ ratio is 71, and therefore, this is only shown in the Supporting Information (Figure S4a). Adding oxalate instead has a significant impact on the speciation equilibrium (Figure 8b). The main complex that is present over a pH range from 1 to 7 is $\text{Fe}(\text{C}_2\text{O}_4)_3^{3-}$. Additionally, the sample pH is shifted to a less acidic range (see Figure 8a,b) where the less photoactive $\text{Fe}(\text{OH})_2^+$ starts to outbalance FeCl_2^+ . A further impact of oxalate in an irradiated system is the scavenging of OH^\bullet , comparable to sulfate.^{34,44}

Concerning catechol, the induced Fe(III) complexes start to occur in a significant fraction as $\text{Fe}(\text{C}_6\text{H}_6\text{O}_2)^+$ at a pH higher than 3 (Supporting Information, Figure S4d). On the other hand, the measured sample pH is lower than 3, where mainly FeCl_2^+ is present. However, during the sample preparation, the salt appeared as dark black, indicating a complex formation with

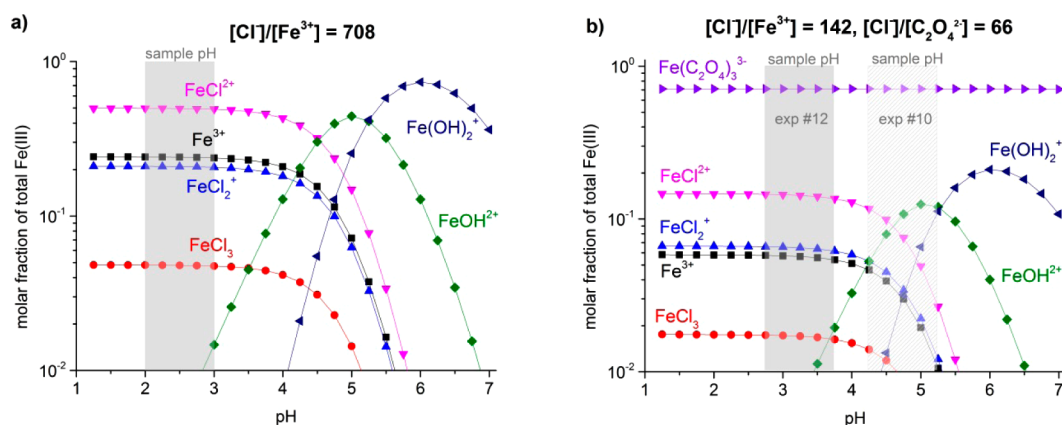


Figure 8. (a,b) Molar fraction of the formed Fe(III) species related to the total Fe(III) content in a saturated sodium chloride solution as a function of the pH (according to the PHREEQC model) for the sample compositions of experiments #7.1–7.5 (a) and experiments #10 and #12. The estimated range of the sample pH based on the measurements described in the text is shown in light gray. Corresponding figures for the other salt compositions are shown in the Supporting Information.

a strong light absorption. Catechol is known to reduce Fe^{3+} to Fe^{2+} at acidic pH^{75,95} and to form extremely stable chelate complexes.⁴⁵ The respective reactions are not included in the speciation model as only Fe(III) complexes are considered. The iron-free sample with catechol and NaCl instead appeared in a light gray color.

In general, the model calculations show that a low pH (<3) induces a large fraction of Fe–Cl complexes and inhibits the photo-Fenton reaction in terms of low OH^\bullet and H_2O_2 production. Thus, a pH of 3 or slightly above would be optimal to warrant the formation of OH^\bullet and thus the reoxidation of the photodecomposed Fe(II)⁹⁵ for a continued, sustainable $\text{Cl}_2^{\bullet-}$ formation via the Fe(III) mechanism.

3.5. Environmental Significance. The influence of soluble iron on speciation and biochemistry plays an important role in nature, for example, in brine-containing soils, intertidal zones, and coastal regions, or where dust or ash aerosols come into contact with sea salt.^{96,97} Recent model predictions extrapolated the present increase of ship traffic into the future and proposed that the soluble iron emitted from ships might contribute 30–60% to the soluble iron deposition in the high-latitude North Atlantic and North Pacific until the year 2100.⁹⁸ Furthermore, Zhu et al.⁹⁹ measured that only 7.5% of the soluble iron in marine aerosol particles is in the lower oxidation state Fe(II), and Schroth et al.¹⁰⁰ confirmed that Fe(III) is predominant, for example, in soil particles from arid regions and in oil combustion products. Our work rather represents halogen release mechanisms above humidified salt sediment as it occurs in salty areas such as the Dead Sea or Australian salt lakes,¹⁰¹ but the proposed mechanisms may also account for iron-containing saline aerosols.

While iron forms mainly complexes with organic ligands in seawater,¹⁰² the situation can change in sea salt aerosols where salinity increases and the pH drops below 2,¹⁰³ and our work indicates an additional potential impact of soluble iron on the atmosphere by the induced intrusion of Cl_2 and Br_2 . The varying content of soluble iron could have affected the tropospheric Cl and Br concentrations in the past. Chlorine is a strong oxidant and is highly reactive with organics having, for example, a 16 times higher reaction rate than OH toward the climate forcing greenhouse gas methane. While it reacts relatively slowly with organics, it leads to surface-level O_3 destruction, mainly initiated by the autocatalytic release of

bromine from sea salt.³⁸ When iron is present together with sea salt, the iron-induced halogen release could complement the classical release mechanisms via O_3 , NO_2 , or N_2O_5 .^{38,104} However, it still remains unclear if the natural iron-induced Cl_2 and Br_2 release plays a relevant role for the halogen activation in the atmosphere, as well as the implications of such rather local events on the global tropospheric chemistry, and, in particular, on variations of the atmospheric methane concentration. In reality, the ratio between the specific reaction surface and the volume in which the halogens are released is much higher in our simulation chamber than that in the affected parts of the atmosphere. The experimental conditions are chosen rather unrealistically (zero air environment and pure salt samples), and the chamber leads to an enrichment of the released gas phase, which helps to better investigate the mechanisms. For more significant conclusions on the environmental impact, aerosol experiments are needed where the specific reaction surface can be measured and the observations are easier to transfer to atmospheric conditions where aerosols have a higher global influence than salt brines.

4. CONCLUSIONS

The chlorine and bromine release from modeled salt pans under simulated solar light in a smog chamber made of Teflon was found to depend on the concentration of iron(III) and inorganic and organic additives. The plain $\text{NaCl}/\text{FeCl}_3 \cdot 6\text{H}_2\text{O}$ samples showed the highest chlorine release. The integrated Cl source in the first hour was about 20 times higher compared to that of the plain NaCl salt pan. The addition of sulfate and oxalate inhibited the activation of chloride significantly by forming complexes and by scavenging Cl atoms and OH radicals in the aqueous phase. Catechol inhibited the Cl_2 release below the detection limit. Adding bromide to the samples led to a slight decrease of released Cl_2 , but simultaneously, a marked bromide activation was observed that increased when Fe(III) was present. This is probably caused by an enrichment of bromide in the QLM and by the drop in pH when Fe(III) is added. In summary, our study demonstrates the photocatalytic effect of Fe(III) causing gaseous Cl production and the influence of inorganic and organic contaminants including the underlying mechanisms that explain the various observed Cl and Br sources.

■ ASSOCIATED CONTENT

■ Supporting Information

Compilation of relevant rate constants for reactions discussed in the text, corresponding figures (production rates, total sources) for the experiments #2, #4, #7.1, #10, and #13, and additional, modeled speciation graphs for experiments #8, #9, #11, and #13. This material is available free of charge via the Internet at <http://pubs.acs.org>.

■ AUTHOR INFORMATION

Corresponding Author

*E-mail: Cornelius.Zetzsch@uni-bayreuth.de. Phone: +49-921-555726.

Notes

The authors declare no competing financial interest.

■ ACKNOWLEDGMENTS

We wish to thank Franz D. Oeste, gM-Ingenieurbüro, Kirchhain, Germany, for advice, Agnes Bednorz and Andrej Einhorn for technical support, and Dr. Gunter Ilgen and Dr. Sarmite Katkevica for the ICP-MS and IC measurements. This work was supported by the DFG within research unit 763 (HALOPROC). S.B. was supported by Ries Consulting, Hosenfeld, Germany.

■ REFERENCES

- (1) Finlayson-Pitts, B. J. Chlorine Atoms as a Potential Tropospheric Oxidant in the Marine Boundary Layer. *Res. Chem. Intermed.* **1993**, *19*, 235–249.
- (2) Spicer, C. W.; Chapman, E. G.; Finlayson-Pitts, B. J.; Platridge, R. A.; Hubbe, J. M.; Fast, J. D.; Berkowitz, C. M. Unexpectedly High Concentrations of Molecular Chlorine in Coastal Air. *Nature* **1998**, *394*, 353–356.
- (3) Platt, U.; Hönninger, G. The Role of Halogen Species in the Troposphere. *Chemosphere* **2003**, *52*, 325–338.
- (4) Osthoff, H. D.; Roberts, J. M.; Ravishankara, A. R.; Williams, E. J.; Lerner, B. M.; Sommariva, R.; Bates, T. S.; Coffman, D.; Quinn, P. K.; Dibb, J. E. High Levels of Nitryl Chloride in the Polluted Subtropical Marine Boundary Layer. *Nat. Geosci.* **2008**, *1*, 324–328.
- (5) Molina, M. J.; Rowland, F. S. Stratospheric Sink for Chlorofluoromethanes: Chlorine Atom-Catalysed Destruction of Ozone. *Nature* **1974**, *249*, 810–812.
- (6) Molina, M. J.; Tso, T.-L.; Molina, L. T.; Wang, F. C. Y. Antarctic Stratospheric Chemistry of Chlorine Nitrate, Hydrogen Chloride, and Ice: Release of Active Chlorine. *Science* **1987**, *238*, 1253–1257.
- (7) von Glasow, R. Atmospheric Chemistry: Wider Role for Airborne Chlorine. *Nature* **2010**, *464*, 168–169.
- (8) Thornton, J. A.; Kercher, J. P.; Riedel, T. P.; Wagner, N. L.; Cozic, J.; Holloway, J. S.; Dubé, W. P.; Wolfe, G. M.; Quinn, P. K.; Middlebrook, A. M. A Large Atomic Chlorine Source Inferred from Mid-Continental Reactive Nitrogen Chemistry. *Nature* **2010**, *464*, 271–274.
- (9) Phillips, G. J.; Tang, M. J.; Thieser, J.; Brickwedde, B.; Schuster, G.; Bohn, B.; Lelieveld, J.; Crowley, J. N. Significant Concentrations of Nitryl Chloride Observed in Rural Continental Europe Associated with the Influence of Sea Salt Chloride and Anthropogenic Emissions. *Geophys. Res. Lett.* **2012**, *39*, L10811.
- (10) Atkinson, R.; Baulch, D. L.; Cox, R. A.; Hampson, R. F.; Kerr, J. A.; Rossi, M. J.; Troe, J. Evaluated Kinetic, Photochemical and Heterogeneous Data for Atmospheric Chemistry: Supplement V. IUPAC Subcommittee on Gas Kinetic Data Evaluation for Atmospheric Chemistry. *J. Phys. Chem. Ref. Data* **1997**, *26*, 521–1011.
- (11) Lowe, D. C.; Allan, W.; Manning, M. R.; Bromley, T.; Brailsford, G.; Ferretti, D.; Gomez, A.; Knobben, R.; Martin, R.; Mei, Z.; et al. Shipboard Determinations of the Distribution of ^{13}C in Atmospheric Methane in the Pacific. *J. Geophys. Res., D* **1999**, *104*, 26125–26135.

(12) Allan, W.; Lowe, D. C.; Caaney, J. M. Active Chlorine in the Remote Marine Boundary Layer: Modeling Anomalous Measurements of $\delta^{13}\text{C}$ in Methane. *Geophys. Res. Lett.* **2001**, *28*, 3239–3242.

(13) Platt, U.; Allan, W.; Lowe, D. Hemispheric Average Cl Atom Concentration from $^{13}\text{C}/^{12}\text{C}$ Ratios in Atmospheric Methane. *Atmos. Chem. Phys.* **2004**, *4*, 2393–2399.

(14) Levine, J. G.; Wolff, E. W.; Jones, A. E.; Sime, L. C. The Role of Atomic Chlorine in Glacial–Interglacial Changes in the Carbon-13 Content of Atmospheric Methane. *Geophys. Res. Lett.* **2011**, *38*, L04801.

(15) Finlayson-Pitts, B. J. Halogens in the Troposphere. *Anal. Chem.* **2009**, *82*, 770–776.

(16) Fickert, S.; Adams, J. W.; Crowley, J. N. Activation of Br_2 and BrCl via Uptake of HOBr onto Aqueous Salt Solutions. *J. Geophys. Res., D* **1999**, *104*, 23719–23727.

(17) Behnke, W.; Elend, M.; Krüger, U.; Zetzsch, C. The Influence of NaBr/NaCl Ratio on the Br^{-2} Catalysed Production of Halogenated Radicals. *J. Atmos. Chem.* **1999**, *34*, 87–99.

(18) Behnke, W.; George, C.; Scheer, V.; Zetzsch, C. Production and Decay of ClNO_2 from the Reaction of Gaseous N_2O_5 with NaCl Solution: Bulk and Aerosol Experiments. *J. Geophys. Res., D* **1997**, *102*, 3795–3804.

(19) Hunt, S. W.; Roeselová, M.; Wang, W.; Wingen, L. M.; Knipping, E. M.; Tobias, D. J.; Dabdub, D.; Finlayson-Pitts, B. J. Formation of Molecular Bromine from the Reaction of Ozone with Deliquesced NaBr Aerosol: Evidence for Interface Chemistry. *J. Phys. Chem. A* **2004**, *108*, 11559–11572.

(20) Jobson, B. T.; Niki, H.; Yokouchi, Y.; Bottenheim, J.; Hopper, F.; Leaitch, R. Measurements of $\text{C}_2\text{--C}_6$ Hydrocarbons During the Polar Sunrise 1992 Experiment: Evidence for Cl Atom and Br Atom Chemistry. *J. Geophys. Res., D* **1994**, *99*, 25355–25368.

(21) Zetzsch, C.; Behnke, W. Heterogeneous Photochemical Sources of Atomic Cl in the Troposphere. *Ber. Bunsen-Ges. Phys. Chem.* **1992**, *96*, 488–493.

(22) Tuckermann, M.; Ackermann, R.; Gözl, C.; Lorenzen-Schmidt, H.; Senne, T.; Stutz, J.; Trost, B.; Unold, W.; Platt, U. DOAS-Observation of Halogen Radical-Catalysed Arctic Boundary Layer Ozone Destruction during the ARCTOC-Campaigns 1995 and 1996 in Ny-Ålesund, Spitsbergen. *Tellus B* **1997**, *49*, 533–555.

(23) Rudolph, J.; Ru, F. B.; Thompson, A.; Anlauf, K.; Bottenheim, J. Halogen Atom Concentrations in the Arctic Troposphere Derived from Hydrocarbon Measurements: Impact on the Budget of Formaldehyde. *Geophys. Res. Lett.* **1999**, *26*, 2941–2944.

(24) Spicer, C. W.; Platridge, R. A.; Foster, K. L.; Finlayson-Pitts, B. J.; Bottenheim, J. W.; Grannas, A. M.; Shepson, P. B. Molecular Halogens before and during Ozone Depletion Events in the Arctic at Polar Sunrise: Concentrations and Sources. *Atmos. Environ.* **2002**, *36*, 2721–2731.

(25) Ramacher, B.; Rudolph, J.; Koppmann, R. Hydrocarbon Measurements in the Spring Arctic Troposphere during the ARCTOC 95 Campaign. *Tellus B* **1997**, *49*, 466–485.

(26) Stutz, J.; Hebestreit, K.; Alicke, B.; Platt, U. Chemistry of Halogen Oxides in the Troposphere: Comparison of Model Calculations with Recent Field Data. *J. Atmos. Chem.* **1999**, *34*, 65–85.

(27) Stutz, J.; Ackermann, R.; Fast, J. D.; Barrie, L. Atmospheric Reactive Chlorine and Bromine at the Great Salt Lake, Utah. *Geophys. Res. Lett.* **2002**, *29*, 18.1–18.4.

(28) Hebestreit, K.; Stutz, J.; Rosen, D.; Matveev, V.; Peleg, M.; Luria, M.; Platt, U. DOAS Measurements of Tropospheric Bromine Oxide in Mid-Latitudes. *Science* **1999**, *283*, 55–57.

(29) Baker, A. K.; Rauthe-Schöch, A.; Schuck, T. J.; Brenninkmeijer, C. A. M.; van Velthoven, P. F. J.; Wisher, A.; Oram, D. E. Investigation of Chlorine Radical Chemistry in the Eyjafjallajökull Volcanic Plume Using Observed Depletions in Non-Methane Hydrocarbons. *Geophys. Res. Lett.* **2011**, *38*, L13801.

(30) Bobrowski, N.; Hönninger, G.; Galle, B.; Platt, U. Detection of Bromine Monoxide in a Volcanic Plume. *Nature* **2003**, *423*, 273–276.

(31) Eder, J. M. Über die Zersetzung des Eisenchlorides und einiger Organischer Ferridsalze im Lichte. *Monatsh. Chem.* **1880**, *1*, 755–762.

- (32) Langford, C. H.; Carey, J. H. The Charge Transfer Photochemistry of the Hexaquoiron (III) Ion, the Chloropentaquoiron (III) Ion, and the μ -Dihydroxo Dimer Explored with tert-Butyl Alcohol Scavenging. *Can. J. Chem.* **1975**, *53*, 2430–2435.
- (33) Nadtochenko, V. A.; Kiwi, J. Photolysis of FeOH^{2+} and FeCl^{2+} in Aqueous Solution. Photodissociation Kinetics and Quantum Yields. *Inorg. Chem.* **1998**, *37*, 5233–5238.
- (34) Machulek, A.; Moraes, J. E. F.; Okano, L. T.; Silverio, C. A.; Quina, F. H. Photolysis of Ferric Ions in the Presence of Sulfate or Chloride Ions: Implications for the Photo-Fenton Process. *Photochem. Photobiol. Sci.* **2009**, *8*, 985–991.
- (35) Machulek, A.; Vautier-Giongo, C.; Moraes, J. E. F.; Nascimento, C. A. O.; Quina, F. H. Laser Flash Photolysis Study of the Photocatalytic Step of the Photo-Fenton Reaction in Saline Solution. *Photochem. Photobiol. Sci.* **2006**, *82*, 208–212.
- (36) Vione, D.; Maurino, V.; Minero, C.; Calza, P.; Pelizzetti, E. Phenol Chlorination and Photochlorination in the Presence of Chloride Ions in Homogeneous Aqueous Solution. *Environ. Sci. Technol.* **2005**, *39*, 5066–5075.
- (37) Lim, M.; Chiang, K.; Amal, R. Photochemical Synthesis of Chlorine Gas from Iron(III) and Chloride Solution. *J. Photochem. Photobiol., A* **2006**, *183*, 126–132.
- (38) Finlayson-Pitts, B. J. The Tropospheric Chemistry of Sea Salt: A Molecular-Level View of the Chemistry of NaCl and NaBr. *Chem. Rev.* **2003**, *103*, 4801–4822.
- (39) Ewing, G. E. H_2O on NaCl: From Single Molecule, to Clusters, to Monolayer, to Thin Film, to Deliquescence; *Intermol Forces Clusters II Struct Bonding 116*; Springer: Berlin, Heidelberg, Germany, 2005.
- (40) Kiwi, J.; Lopez, A.; Nadtochenko, V. Mechanism and Kinetics of the OH-Radical Intervention during Fenton Oxidation in the Presence of a Significant Amount of Radical Scavenger (Cl^-). *Environ. Sci. Technol.* **2000**, *34*, 2162–2168.
- (41) Moorhead, E. G.; Sutin, N. Rate and Equilibrium Constants for the Formation of the Monooxalate Complex of Iron(III). *Inorg. Chem.* **1966**, *5*, 1866–1871.
- (42) Mentasti, E.; Pelizzetti, E. Reactions Between Iron(III) and Catechol (o-Dihydroxybenzene). Part I. Equilibria and Kinetics of Complex Formation in Aqueous Acid Solution. *J. Chem. Soc., Dalton Trans.* **1973**, *23*, 2605–2608.
- (43) Weller, C.; Tilgner, A.; Bräuer, P.; Herrmann, H. Modeling the Impact of Iron–Carboxylate Photochemistry on Radical Budget and Carboxylate Degradation in Cloud Droplets and Particles. *Environ. Sci. Technol.* **2014**, *48*, 5652–5659.
- (44) Balmer, M. E.; Sulzberger, B. Atrazine Degradation in Irradiated Iron/Oxalate Systems: Effects of pH and Oxalate. *Environ. Sci. Technol.* **1999**, *33*, 2418–2424.
- (45) Hider, R. C.; Mohd-Nor, A. R.; Silver, J.; Morrison, I. E. G.; Rees, L. V. C. Model Compounds for Microbial Iron-Transport Compounds. Part I. Solution Chemistry and Mossbauer Study of Iron(II) and Iron(III) Complexes from Phenolic and Catecholic Systems. *J. Chem. Soc., Dalton Trans.* **1981**, *2*, 609–622.
- (46) Tofan-Lazar, J.; Al-Abadleh, H. A. Surface Water Enhances the Uptake and Photoreactivity of Gaseous Catechol on Solid Iron(III) Chloride. *Environ. Sci. Technol.* **2013**, 394–402.
- (47) Buxmann, J.; Balzer, N.; Bleicher, S.; Platt, U.; Zetzsch, C. Observations of Bromine Explosions in Smog Chamber Experiments above a Model Salt Pan. *Int. J. Chem. Kinet.* **2012**, *44*, 312–326.
- (48) Bleicher, S.; Buxmann, J. C.; Sander, R.; Riedel, T. P.; Thornton, J. A.; Platt, U.; Zetzsch, C. The Influence of Nitrogen Oxides on the Activation of Bromide and Chloride in Salt Aerosol. *Atmos. Chem. Phys. Discuss.* **2014**, *14*, 10135–10166.
- (49) Flynn, C. M. Hydrolysis of Inorganic Iron(III) Salts. *Chem. Rev.* **1984**, *84*, 31–41.
- (50) Behnke, W.; Holländer, W.; Koch, W.; Nolting, F.; Zetzsch, C. A Smog Chamber for Studies of the Photochemical Degradation of Chemicals in the Presence of Aerosols. *Atmos. Environ.* **1988**, *22*, 1113–1120.
- (51) Zetzsch, C.; Behnke, W. Heterogeneous Reactions of Chlorine Compounds. In *The Tropospheric Chemistry of Ozone in the Polar Regions*; Niki, H., Becker, K., Eds.; NATO ASI Series; Springer: Berlin, Heidelberg, Germany, 1993; pp 291–306.
- (52) Zangmeister, C. D.; Turner, J. A.; Pemberton, J. E. Segregation of NaBr in NaBr/NaCl Crystals Grown from Aqueous Solutions: Implications for Sea Salt Surface Chemistry. *Geophys. Res. Lett.* **2001**, *28*, 995–998.
- (53) Rossi, M. J. Heterogeneous Reactions on Salts. *Chem. Rev.* **2003**, *103*, 4823–4882.
- (54) Scheer, V.; Frenzel, A.; Behnke, W.; Zetzsch, C.; Magi, L.; George, C. Mirabel, P. Uptake of Nitrosyl Chloride (NOCl) by Aqueous Solutions. *J. Phys. Chem. A* **1997**, *101*, 9359–9366.
- (55) Carter, W. P. L. Measurement and Modeling of NO_x Offgassing from FEP Teflon Chambers. *Proceedings of Sixth US/Germany Workshop on Ozone/Fine Particle*; Riverside California, October 4–6 1999.
- (56) Park, J.-H.; Christov, C. I.; Ivanov, A. V.; Molina, M. J.; On, O. H. Uptake by Sea Salt under Humid Conditions. *Geophys. Res. Lett.* **2009**, *36*, L02802.
- (57) Hirokawa, J.; Onaka, K.; Kajii, Y.; Akimoto, H. Heterogeneous Processes Involving Sodium Halide Particles and Ozone: Molecular Bromine Release in the Marine Boundary Layer in the Absence of Nitrogen Oxides. *Geophys. Res. Lett.* **1998**, *25*, 2449–2452.
- (58) Mochida, M.; Akimoto, H.; van den Bergh, H.; Rossi, M. J. Heterogeneous Kinetics of the Uptake of HOBr on Solid Alkali Metal Halides at Ambient Temperature. *J. Phys. Chem. A* **1998**, *102*, 4819–4828.
- (59) Oum, K. W.; Lakin, M. J.; DeHaan, D. O.; Brauers, T.; Finlayson-Pitts, B. J. Formation of Molecular Chlorine from the Photolysis of Ozone and Aqueous Sea-Salt Particles. *Science* **1998**, *279*, 74–76.
- (60) Park, J.-H.; Ivanov, A. V.; Molina, M. J. Effect of Relative Humidity on OH Uptake by Surfaces of Atmospheric Importance. *J. Phys. Chem. A* **2008**, *112*, 6968–6977.
- (61) Park, J.-H.; Ivanov, A. V.; Molina, M. J. Experimental Study on the Release of Cl_2 from NaCl upon OH Radical Uptake. *Microchem. J.* **2013**, *110*, 695–701.
- (62) Frinak, E. K.; Abbatt, J. P. D. Br_2 Production from the Heterogeneous Reaction of Gas-Phase OH with Aqueous Salt Solutions: Impacts of Acidity, Halide Concentration, and Organic Surfactants. *J. Phys. Chem. A* **2006**, *110*, 10456–10464.
- (63) Nissenon, P.; Wingen, L. M.; Hunt, S. W.; Finlayson-Pitts, B. J.; Dabdub, D. Rapid Formation of Molecular Bromine from Deliquesced NaBr Aerosol in the Presence of Ozone and UV Light. *Atmos. Environ.* **2014**, *89*, 491–506.
- (64) Yu, X.-Y. Critical Evaluation of Rate Constants and Equilibrium Constants of Hydrogen Peroxide Photolysis in Acidic Aqueous Solutions Containing Chloride Ions. *J. Phys. Chem. Ref. Data* **2004**, *33*, 747–763.
- (65) Elliot, A. J. A Pulse Radiolysis Study of the Temperature Dependence of Reactions Involving H, OH and e^-_{aq} in Aqueous Solutions. *Radiat. Phys. Chem.* **1989**, *34*, 753–758.
- (66) Zimmerman, G.; Strong, F. C. Equilibria and Spectra of Aqueous Chlorine Solutions. *J. Am. Chem. Soc.* **1957**, *79*, 2063–2066.
- (67) Jayson, G. G.; Parsons, B. J.; Swallow, A. J. Some Simple, Highly Reactive, Inorganic Chlorine Derivatives in Aqueous Solution. Their Formation Using Pulses of Radiation and their Role in the Mechanism of the Fricke Dosimeter. *J. Chem. Soc., Faraday Trans. 1* **1973**, *69*, 1597–1607.
- (68) Thornton, A. T.; Laurence, G. S. Kinetics of Oxidation of Transition-Metal Ions by Halogen Radical Anions. Part I. The oxidation of Iron(II) by Dibromide and Dichloride Ions Generated by Flash Photolysis. *J. Chem. Soc., Dalton Trans.* **1973**, *8*, 804–813.
- (69) de Laat, J.; Le, T. G. Kinetics and Modeling of the $\text{Fe(III)/H}_2\text{O}_2$ System in the Presence of Sulfate in Acidic Aqueous Solutions. *Environ. Sci. Technol.* **2005**, *39*, 1811–1818.
- (70) King, W.; Aldrich, R. A.; Charnecki, S. E. Photochemical Redox Cycling of Iron in NaCl Solutions. *Mar. Chem.* **1993**, *44*, 105–120.

- (71) Sander, R. *Compilation of Henry's Law Constants for Inorganic and Organic Species of Potential Importance in Environmental Chemistry*, version 3. <http://www.henrys-law.org/henry.pdf> (1999).
- (72) Byrne, R. H.; Kester, D. R. Ultraviolet Spectroscopic Study of Ferric Equilibria at High Chloride Concentrations. *J. Solution Chem.* **1981**, *10*, 51–67.
- (73) Nadochenko, V.; Kiwi, J. Primary Photochemical Reactions in the Photo-Fenton System with Ferric Chloride. 1. A Case Study of Xylidine Oxidation as a Model Compound. *Environ. Sci. Technol.* **1998**, *32*, 3273–3281.
- (74) de Laat, J.; Le, T. G.; Legube, B. A Comparative Study of the Effects of Chloride, Sulfate and Nitrate Ions on the Rates of Decomposition of H₂O₂ and Organic Compounds by Fe(II)/H₂O₂ and Fe(III)/H₂O₂. *Chemosphere* **2004**, *55*, 715–723.
- (75) Pracht, J.; Boenigk, J.; Isenbeck-Schröder, M.; Keppler, F.; Schöler, H. F. Abiotic Fe(III) Induced Mineralization of Phenolic Substances. *Chemosphere* **2001**, *44*, 613–619.
- (76) Zuo, Y.; Hoigné, J. Formation of Hydrogen Peroxide and Depletion of Oxalic Acid in Atmospheric Water by Photolysis of Iron(III)–Oxalato Complexes. *Environ. Sci. Technol.* **1992**, *26*, 1014–1022.
- (77) Mochida, M.; Hirokawa, J.; Kajii, Y.; Akimoto, H. Heterogeneous Reactions of Cl₂ with Sea Salts at Ambient Temperature: Implications for Halogen Exchange in the Atmosphere. *Geophys. Res. Lett.* **1998**, *25*, 3927–3930.
- (78) Sadanaga, Y.; Hirokawa, J.; Akimoto, H. Formation of Molecular Chlorine in Dark Condition: Heterogeneous Reaction of Ozone with Sea Salt in the Presence of Ferric Ion. *Geophys. Res. Lett.* **2001**, *28*, 4433–4436.
- (79) Baes, C. F.; Mesmer, R. E. *The Hydrolysis of Cations*; Wiley: New York, 1976.
- (80) Kester, D. R.; Byrne, R. H.; Liang, Y.-J. Redox Reactions and Solution Complexes of Iron in Marine Systems. In: *Marine Chemistry in the Coastal Environment*; Church, T. M., Ed.; American Chemical Society: Washington, DC, 1975; Vol. 18, pp 56–79.
- (81) Martell, A. E.; Smith, R. M. *Critical Stability Constants. Vol. 4. Inorganic Complexes*; Plenum: New York, 1976.
- (82) Yatsimirskii, K. B.; Vasil'ev, V. P. *Instability Constants of Complex Compounds*; Pergamon Press: Oxford, U.K., 1960.
- (83) Lister, M. W.; Rivington, D. E. Some Ferric Halide Complexes, and Ternary Complexes with Thiocyanate Ions. *Can. J. Chem.* **1955**, *33*, 1603–1613.
- (84) Avdeef, A.; Sofen, S. R.; Bregante, T. L.; Raymond, K. N. Coordination Chemistry of Microbial Iron Transport Compounds. 9. Stability Constants for Catechol Models of Enterobactin. *J. Am. Chem. Soc.* **1978**, *100*, 5362–5370.
- (85) Parkhurst, D. L.; Appelo, C. A. *User's Guide to PHREEQC (Version 2): A Computer Program for Speciation, Batch-Reaction, One-Dimensional Transport, and Inverse Geochemical Calculations*; U.S. Geological Survey: Washington, DC, 1999.
- (86) Allison, J. D.; Brown, D. S.; Kevin, J. *MINTEQA2/PRODEFA2, A Geochemical Assessment Model for Environmental Systems: Version 3.0 User's Manual*; Environmental Research Laboratory, Office of Research and Development, U.S. Environmental Protection Agency: Athens, GA, 1991.
- (87) Pitzer, K. S. Thermodynamics of Electrolytes. I. Theoretical Basis and General Equations. *J. Phys. Chem.* **1973**, *77*, 268–277.
- (88) Tosca, N. J.; McLennan, S. M.; Clark, B. C.; Grotzinger, J. P.; Hurowitz, J. A.; Knoll, A. H.; Schröder, C.; Squyres, S. W. Geochemical Modeling of Evaporation Processes on Mars: Insight from the Sedimentary Record at Meridiani Planum. *Earth Planet. Sci. Lett.* **2005**, *240*, 122–148.
- (89) Hüchel, E. Zur Theorie konzentrierter wässriger Lösungen starker Elektrolyte. *Phys. Z.* **1925**, *26*, 93–147.
- (90) Truesdell, A. H.; Jones, B. F. *WATEQ, A Computer Program for Calculating Chemical Equilibria of Natural Waters*; U.S. Department of the Interior, Geological Survey: Washington, DC, 1973.
- (91) Crowe, A. S., Longstaffe, F. J., Eds. *Extension of Geochemical Modelling Techniques to Brines: Coupling of the Pitzer Equations to PHREEQC*; Department of Geology, University of Alberta: Edmonton, Canada; 1987; Vol. 1.
- (92) Merkel, B.; Planer-Friedrich, B. *Groundwater Geochemistry: A Practical Guide to Modeling of Natural and Contaminated Aquatic Systems*; Springer: Berlin, Heidelberg, Germany, 2008.
- (93) Pitzer, K. S. Thermodynamics of Electrolytes. I. Theoretical Basis and General Equations. *J. Phys. Chem.* **1973**, *77*, 268–277.
- (94) Rabinowitch, E.; Stockmayer, W. H. Association of Ferric Ions with Chloride, Bromide and Hydroxyl Ions (A Spectroscopic Study). *J. Am. Chem. Soc.* **1942**, *64*, 335–347.
- (95) Machulek, A.; Moraes, J. E. F.; Vautier-Giongo, C.; Silverio, C. A.; Friedrich, L. C.; Nascimento, C. A. O.; Gonzalez, M. C.; Quina, F. H. Abatement of the Inhibitory Effect of Chloride Anions on the Photo-Fenton Process. *Environ. Sci. Technol.* **2007**, *41*, 8459–8463.
- (96) Spolaor, A.; Vallelonga, P.; Cozzi, G.; Gabrieli, J.; Varin, C.; Kehrwald, N.; Zennaro, P.; Boutron, C.; Barbante, C. Iron Speciation in Aerosol Dust Influences Iron Bioavailability over Glacial–Interglacial Timescales. *Geophys. Res. Lett.* **2013**, *40*, 1618–1623.
- (97) Mahowald, N. M.; Engelstaedter, S.; Luo, C.; Sealy, A.; Artaxo, P.; Benitez-Nelson, C.; Bonnet, S.; Chen, Y.; Chuang, P. Y.; Cohen, D. D. Atmospheric Iron Deposition: Global Distribution, Variability, and Human Perturbations. *Annu. Rev. Mar. Sci.* **2009**, *1*, 245–278.
- (98) Ito, A. Global Modeling Study of Potentially Bioavailable Iron Input from Shipboard Aerosol Sources to the Ocean. *Global Biogeochem. Cycles* **2013**, *27*, 1–10.
- (99) Zhu, X.; Prospero, J. M.; Savoie, D. L.; Millero, F. J.; Zika, R. G.; Saltzman, E. S. Photoreduction of Iron(III) in Marine Mineral Aerosol Solutions. *J. Geophys. Res., D* **1993**, *98*, 9039–9046.
- (100) Schroth, A. W.; Crusius, J.; Sholkovitz, E. R.; Bostick, B. C. Iron Solubility Driven by Speciation in Dust Sources to the Ocean. *Nat. Geosci.* **2009**, *2*, 337–340.
- (101) Krause, T.; Tubbesing, C.; Benzing, K.; Schöler, H. F. Model Reactions and Natural Occurrence of Furans from Hypersaline Environments. *Biogeosci. Discuss.* **2013**, *10*, 17439–17468.
- (102) Rue, E. L.; Bruland, K. W. Complexation of Iron(III) by Natural Organic Ligands in the Central North Pacific as Determined by a New Competitive Ligand Equilibration/Adsorptive Cathodic Stripping Voltammetric Method. *Mar. Chem.* **1995**, *50*, 117–138.
- (103) Zhu, X.; Prospero, J. M.; Millero, F. J.; Savoie, D. L.; Brass, G. W. The Solubility of Ferric Ion in Marine Mineral Aerosol Solutions at Ambient Relative Humidities. *Mar. Chem.* **1992**, *38*, 91–107.
- (104) Finlayson-Pitts, B. J.; Ezell, M. J.; Pitts, J. N. Formation of Chemically Active Chlorine Compounds by Reactions of Atmospheric NaCl Particles with Gaseous N₂O₃ and ClONO₂. *Nature* **1989**, *337*, 241–244.